INTERNATIONAL JOURNAL FOR NUMERICAL METHODS IN ENGINEERING
Int. J. Numer. Meth. Engng 2013; **00**:1–20
Published online in Wiley InterScience (www.interscience.wiley.com). DOI: 10.1002/nme

A fast weakly-intrusive multiscale method in explicit dynamics

IJNME, Volume 100, Issue 8, pages 577595, 23 November 2014, DOI: 10.1002/nme.4750

Omar Bettinotti[1,4], Olivier Allix[1], Umberto Perego[2], Victor Oancea [3], Benoît Malherbe [4]

[1] *LMT-Cachan, ENS-Cachan/CNRS/Pres UniverSud Paris, 61 avenue du President Wilson, 94235 Cachan, France.*
[2] *Department of Civil and Environmental Engineering, Politecnico di Milano, P.zza L. da Vinci, 32, 20133 Milano, Italy.*
[3] *R&D Dassault Systèmes Simulia, CTO Office, 166 Valley Street, 02909-2499 Providence RI, United States.*
[4] *Airbus Operations SAS, Vulnerability Tech Center, 316 Route de Bayonne, 31060 Toulouse, France.*

SUMMARY

This paper presents new developments on a weakly-intrusive approach for the simplified implementation of space and time multiscale methods within an explicit dynamics software. The "substitution" method proposed in previous works allows to take advantage of a global coarse model, typically used in an industrial context, running separate, refined in space and in time, local analyses only where needed. The proposed technique is iterative, but the explicit character of the method allows to perform the global computation only once per global time step, while a repeated solution is required for the small local problems only. Nevertheless, a desirable goal is to reach convergence with a reduced number of iterations. To this purpose, we propose here a new iterative algorithm based on an improved interface inertia operator. The new operator exploits a combined property of velocity Hermite time interpolation on the interface and of the central difference integration scheme, allowing the consistent upscaling of interface inertia contributions from the lower scale. This property is exploited to construct an improved mass matrix operator for the interface coupling, allowing to significantly enhance the convergence rate. The efficiency and robustness of the procedure is demonstrated through several examples of growing complexity.

Received . . .

KEY WORDS: global-local coupling; substitution method; explicit dynamics; multi-time-step analysis; non-intrusive technique

1. INTRODUCTION

When dealing with large problems, a common engineering practice is to start by a global (macroscale) analysis of the structure in order to localize the potential area of stress concentration, possibly giving rise to non-linearity and failure. The problem is then re-analyzed. A first approach is to define an updated finite element model taking into account nonlinearity and fine structural details, and to run the full model again. Nevertheless, this procedure can be very costly and, therefore, sub-modeling is often used. The method consists in a re-analysis of the local (microscale) area of interest, to which suitable boundary conditions, deduced from the global analysis, are applied. Although widely available in commercial codes and numerically efficient, sub-modeling suffers from a strong limitation: it ignores the effect of the local response on the global structural behavior. As a consequence, it cannot assess phenomena such as stress redistributions and tend to introduce uncontrolled errors due to the inaccuracy of local boundary conditions. This is one of the reasons

*Correspondence to: LMT-Cachan, ENS-Cachan/CNRS/Pres UniverSud Paris, 61 avenue du Président Wilson, 94235 Cachan, France. E-mail: bettinotti@lmt.ens-cachan.fr

why concurrent multiscale methods in space [1, 2, 3, 4, 5] but also in time [6, 7] have been the subject of intensive research in recent years. To deal with damage and delamination, which is one of the motivations of this work in the case of impact [8], specific extensions of previous multiscale approaches have been developed [9, 10, 11, 12, 13].

In the case of dynamics, monolithic strategies were first proposed (e.g. implicit-explicit algorithms [14, 15] or multi-time-step methods [16, 17]). More recently, non-overlapping dual domain decomposition methods [18, 19, 20], mixed [21] or overlapping methods like in the Arlequin framework [22] have been developed. A quite demanding aspect of those methods is the need to partition the global mesh and to establish interface conditions between adjacent subdomains. This is usually a complex operation to be implemented in a commercial code, often requiring a substantial modification of the code architecture (for this reason we use the word "intrusive"). Moreover, this operation should be performed a large number of times in the case of problems where the domain to be refined evolves in time.

The main goal of the non-intrusive approach proposed in [23], which will be hereafter referred to as "substitution" method, is to avoid this operation, though at the price of iterations. The approach is said to be non-intrusive, because data exchanges between the global analysis and the locally refined one concern only nodal velocities and forces at the interface, quantities which are easily accessible in commercial codes. The versatility of the approach is such that, in principle, different codes could be used to solve the problems defined at the different scales. The method has already proved its efficiency in allowing the use in commercial finite element codes of advanced techniques such as, e.g., XFEM [24].

First developed in statics, non-intrusive approaches have attracted attention also in dynamics. For example, for thermal shock problems [25, 26], a non-intrusive version of the Generalized Finite Element Method (GFEM) was proposed. Recently, a proposal for simplifying the use of the non-overlapping dual domain decomposition methods [19] in the case where two different codes are used was presented in [27]. The search of non-intrusivity is in this case focused on the programming of data exchanges between the two codes.

As in statics, the dynamics version [28] of the substitution method consists of an iterative coupling between a global analysis of the entire structure and a refined local analysis restricted to the regions of interest. An appealing feature of the proposed approach in explicit dynamics is that the global problem analysis has to be performed only once per global time step. Iterations have to been carried out only on the local region of interest. This is in contrast to the implicit case, where iterations involve repeated global analyses. This is for example the case of global-local approaches [29, 30] which motivates the development of non-intrusive acceleration techniques [31, 24].

The iterative process is substantially different in statics and in explicit dynamics. In the latter case, conditional stability of the time integration scheme requires very small time steps and the number of operations to be carried out at each time step turns out to be critical from the computational standpoint. Therefore the number of iterations has to be kept as small as possible, which is the concern of this paper. To this purpose, the fixed point algorithm proposed in [28] has been revisited and improved in two aspects. The first one consists of an improved initialization of the time step algorithm, taking into account the result of the previous global time step. This always allows to reduce the number of iterations, up to a factor of two, depending on the test case. The second aspect concerns a new definition of the inertia interface operator, which is the core of the paper.

The inertia interface operator carries interface information from the micro- to the macro-scale and its definition is based on a peculiar property of the time interpolation scheme of the interface velocities. In [28] it was shown that a stable formulation could be achieved through a Hermite interpolation in time of the interface macroscale velocities. This implied to express interface velocities in terms of velocities and accelerations at the beginning and at the end of the global time step. In this paper we show that assigning velocities interpolated in this way as boundary conditions on the local problem implies that not only velocities, but also accelerations on the interface coincide at the local and global scale at the end of the global time step. The fact that inertia forces at the local and global scale originate from identical acceleration histories, allows to derive an inertia interface operator (in other words a modified mass matrix) at the global scale, implementing the coupling

DOI: 10.1002/nme

between the two scales in a way consistent with the adopted time and space discretization. When using this operator, the rate of convergence is roughly increased by a factor 3, leading to a reduced number of iterations per global time step, usually between 1 and 3 for the different tests conducted so far.

The paper is organized as follows. In Section 2, the algebraic reference multiscale problem is formulated. The time and space up-scaling and down-scaling operators are introduced. Then the acceleration compatibility property across the scales is derived. Since communication between the scales takes place at the interface between the region of interest and the rest of the structure, special attention is devoted to the derivation of the interface conditions, which are at the foundation of the problem formulation. In Section 3, the main concepts of the substitution methods are presented along with the equations to be satisfied by the method. In Section 4, the associated iterative scheme is described. Section 5 is devoted to examples of various nature obtained by means of a Matlab prototype. In the first example, results obtained with the proposed scheme are compared to those obtained using the algorithm presented in [28]. Then the method is applied to two other types of problems. In the first type, inhomogeneities not considered in the global model are introduced in the local problem. The results confirm the robustness of the method also in cases where the global model is far to be equivalent to the local one. The last example concerns the propagation of delamination, showing the possibility to use the method in an adaptive way, keeping the same global model and varying the definition of the local problem, depending on the history of deformation of the structure.

2. REFERENCE PROBLEM

For the presentation of the method, use will be made of a problem of the type shown in Figure 1, which will be referred to as the "reference problem". It consists of a simple structure composed of two parts. The part on the left, referred to in what follows as the "local" region and denoted by Ω_ℓ, is characterized by fine features, such as, e.g., small geometric details, microvoids or microcracks, highly localized loading conditions, structured material and so on, which require a fine resolution both in time and in space. The part on the right, referred to as the "complementary" part and denoted by Ω_c, requires only a coarse resolution, both in space and in time, such as in the case of regular geometry, smoothly distributed loading, homogeneous material.

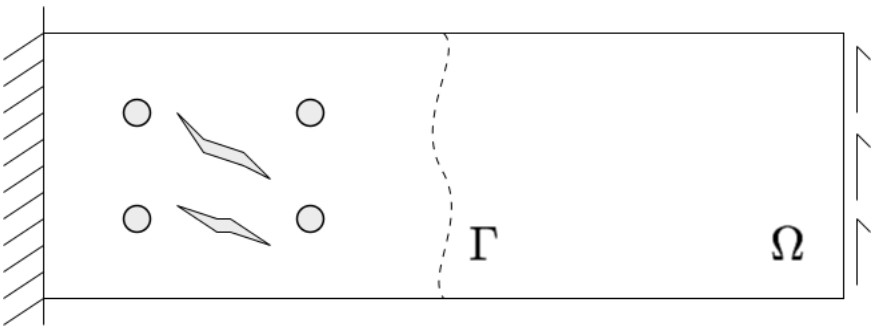

Figure 1. Structural problem to be analyzed, exhibiting two geometric and temporal scales.

We assume that the problem has been discretized using a displacement-based finite element method using a heterogeneous mesh. The fine mesh, referred to as "local mesh", is constructed in such a way that the nodes on Γ of the coarse mesh, referred to as "complementary mesh", are always matched by a corresponding node of the local mesh in Figure 2.

The problem is solved integrating the motion using an explicit central difference scheme. The different time scales of the two regions require different time steps to properly resolve the dominant frequencies of each region. Furthermore, since only conditional stability is guaranteed by the central difference method, the smaller mesh size leads to a smaller critical time step. We define Δt_ℓ and Δt_c

DOI: 10.1002/nme

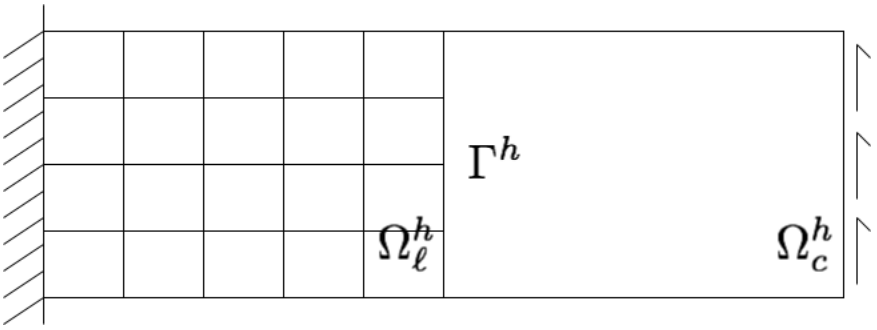

(a) *spatial mesh*

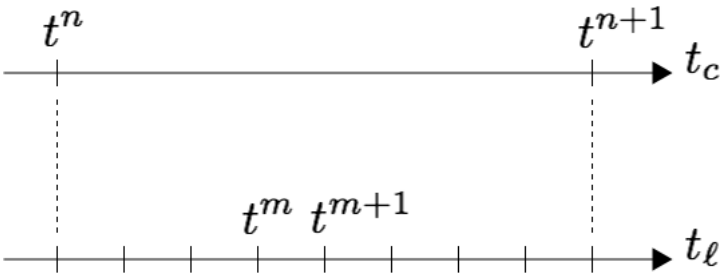

(b) *temporal discretization*

Figure 2. Heterogeneous discretization in space and time of reference problem.

the time steps used in the two regions. Although not required, in order to simplify the discussion, they are chosen such that $\Delta t_c = M\Delta t_\ell$, where M is a integer greater than 1 (Figure 2).

2.1. Space and time down- and up-scaling operators and associated properties

Kinematic compatibility along the interface Γ between the two regions is enforced at the nodes of the coarse mesh. Velocities of the remaining nodes of the local mesh on Γ are obtained by means of linear interpolation of velocities of the nodes of the complementary mesh. Denoting by $\mathbf{V}_{\ell,\Gamma}$ and $\mathbf{V}_{c,\Gamma}$ velocities at nodes of the local and complementary meshes, respectively, on Γ, we set

$$\mathbf{V}_{\ell,\Gamma} = \Pi_h^1 \mathbf{V}_{c,\Gamma} \tag{1}$$

where Π_h^1 is the downscaling spatial operator enforcing the compatibility condition at the interface between local and complementary regions. The 1 at the exponent denotes the linear spatial interpolation between nodes of the coarse mesh.

As in [28] time compatibility is enforced on Γ through Hermite interpolation of complementary velocities $\mathbf{V}_{c,\Gamma}$ and accelerations $\mathbf{A}_{c,\Gamma}$. Let us consider a time step Δt_c going from the macroscopic time t^n to $t^{n+1} = t^n + \Delta t_c$. Let $t^m = t^n + m\Delta t_\ell$, $0 \leq m \leq M$, be a generic time point at the local time scale, within the same macroscopic time step. One can write

$${}^{m+1}\mathbf{V}_{\ell,\Gamma} = \Pi_h^1 \Pi_t^3 \left({}^n\mathbf{V}_{c,\Gamma}, {}^{n+1}\mathbf{V}_{c,\Gamma}, {}^n\mathbf{A}_{c,\Gamma}, {}^{n+1}\mathbf{A}_{c,\Gamma}\right) \tag{2}$$

where Π_t^3 is the Hermite interpolation operator, which in this case plays the role of downscaling time operator, allowing to express the local velocities on Γ $\mathbf{V}_{\ell,\Gamma}(t)$ as a cubic function of time.

Remark 1
Velocities at times t^n or t^{n+1} are not usually calculated in commercial finite element codes based on the central difference scheme, but they can be defined in function of mid-step velocities and current

DOI: 10.1002/nme

accelerations as

$$\begin{aligned} {}^{m}\mathbf{V}_{c,\Gamma} &= {}^{n-\frac{1}{2}}\mathbf{V}_{c,\Gamma} + \frac{\Delta t_c}{2}\,{}^{n}\mathbf{A}_{c,\Gamma} \\ {}^{n+1}\mathbf{V}_{c,\Gamma} &= {}^{n+\frac{1}{2}}\mathbf{V}_{c,\Gamma} + \frac{\Delta t_c}{2}\,{}^{n+1}\mathbf{A}_{c,\Gamma} \\ {}^{m+1}\mathbf{V}_{\ell,\Gamma} &= {}^{m+\frac{1}{2}}\mathbf{V}_{\ell,\Gamma} + \frac{\Delta t_\ell}{2}\,{}^{m+1}\mathbf{A}_{\ell,\Gamma} \end{aligned} \tag{3}$$

Let us note, for instance, that within the Abaqus software the velocities at t^{n+1} are available when some options of the so-called "Co-Simulation technique" are activated.

Let $s(t) = (t - t^n)/\Delta t_c$, $0 \le s \le 1$, $t^n \le t \le t^{n+1}$, be an intrinsic local time. Hermite interpolation allows to write

$$\begin{aligned} \mathbf{V}_{\ell,\Gamma}(s) = (1 - 3s^2 + 2s^3)\Pi_h^1({}^{n}\mathbf{V}_{c,\Gamma}) + \Delta t_c(s - 2s^2 + s^3)\Pi_h^1({}^{n}\mathbf{A}_{c,\Gamma}) \\ +(3s^2 - 2s^3)\Pi_h^1({}^{n+1}\mathbf{V}_{c,\Gamma}) + \Delta t_c(-s^2 + s^3)\Pi_h^1({}^{n+1}\mathbf{A}_{c,\Gamma}) \end{aligned} \tag{4}$$

Hermite interpolation was used in [28] rather than linear interpolation since it was shown that linear interpolation would lead to numerical instability of the local accelerations along the interface.

Hermite interpolation of interface velocities, when used in conjunction with a central difference scheme at both scales, exhibits an additional important property which was not noticed in previous works. According to the central difference scheme, velocities at the end of a time step are expressed in terms of accelerations at the two scales as

$$\begin{aligned} {}^{n+1}\mathbf{V}_{c,\Gamma} &= {}^{n}\mathbf{V}_{c,\Gamma} + \frac{\Delta t_c}{2}({}^{n}\mathbf{A}_{c,\Gamma} + {}^{n+1}\mathbf{A}_{c,\Gamma}) \\ {}^{m+1}\mathbf{V}_{\ell,\Gamma} &= {}^{m}\mathbf{V}_{\ell,\Gamma} + \frac{\Delta t_\ell}{2}({}^{m}\mathbf{A}_{\ell,\Gamma} + {}^{m+1}\mathbf{A}_{\ell,\Gamma}) \end{aligned} \tag{5}$$

The first of Equations (5) shows that ${}^{n+1}\mathbf{V}_{c,\Gamma}$ is not an independent parameter in (4) and it can be eliminated from (4) expressing it in terms of the other three parameters. If the first of the (5) is substituted in (4), one obtains

$$\mathbf{V}_{\ell,\Gamma}(s) = \Pi_h^1({}^{n}\mathbf{V}_{c,\Gamma}) + \Delta t_c s\,\Pi_h^1({}^{n}\mathbf{A}_{c,\Gamma}) + \Delta t_c \frac{s^2}{2}\Pi_h^1({}^{n+1}\mathbf{A}_{c,\Gamma} - {}^{n}\mathbf{A}_{c,\Gamma}) \tag{6}$$

which reveals that a quadratic evolution of interface velocities is actually enforced at the lower scale.

We are able now to show that the accelerations on the interface at the local time steps, as obtained by the application of the central difference scheme, have the following expression:

$${}^{m}\mathbf{A}_{\ell,\Gamma} = \left(1 - \frac{m}{M}\right)\Pi_h^1({}^{n}\mathbf{A}_{c,\Gamma}) + \frac{m}{M}\Pi_h^1({}^{n+1}\mathbf{A}_{c,\Gamma}) \tag{7}$$

This in turns implies that the accelerations obtained by the proposed numerical scheme coincide at each local time step with the expression of the derivative of the velocities on the interface (6) with respect to time at each local time step. This result, which could appear as trivial at first, is in general not valid for a Newmark scheme and for the central difference scheme either. It is only the peculiar expression of the prescribed velocities at the interface which ensures this property which therefore has to be proven. More important this also implies that the local and global accelerations on the interface coincide at each global time step i.e. at $m = M$. Let us note that it is not the case in multiscale methods in time where the connection at the interface is made by assuming the equality of velocities which in general, does not imply the equality of the accelerations on the interface.

Expression (7) is valid for $m = 0$ that is ${}^{0}\mathbf{A}_{\ell,\Gamma} = \Pi_h^1({}^{n}\mathbf{A}_{c,\Gamma})$. This either follows from the initial condition ${}^{0}\mathbf{A}_{\ell,\Gamma} = \mathbf{0}$ and ${}^{0}\mathbf{A}_{c,\Gamma} = \mathbf{0}$ or is prescribed when the local region is activated in the analysis at a given global time step.

At the local level the central is applied. Therefore, from (5), noting that $s(t^m) = m\Delta t_\ell/\Delta t_c$, it follows:

$${}^{m}\mathbf{A}_{\ell,\Gamma} + {}^{m+1}\mathbf{A}_{\ell,\Gamma} = \frac{2}{\Delta t_\ell}({}^{m+1}\mathbf{V}_{\ell,\Gamma} - {}^{m}\mathbf{V}_{\ell,\Gamma}) \tag{8}$$

DOI: 10.1002/nme

Taking into account the expression of the velocities on the interface (6) in the previous expression (8) leads to:

$$ {}^{m}\mathbf{A}_{\ell,\Gamma} + {}^{m+1}\mathbf{A}_{\ell,\Gamma} = 2\Pi_h^1({}^{n}\mathbf{A}_{c,\Gamma}) + \frac{2m+1}{M}\Pi_h^1({}^{n+1}\mathbf{A}_{c,\Gamma} - {}^{n}\mathbf{A}_{c,\Gamma}) \tag{9} $$

Assuming that the relation (7) is valid for a given m and introducing this expression of the acceleration at m in the previous relation (9), it follows:

$$ {}^{m+1}\mathbf{A}_{\ell,\Gamma} = \left(1 - \frac{m+1}{M}\right)\Pi_h^1({}^{n}\mathbf{A}_{c,\Gamma}) + \frac{m+1}{M}\Pi_h^1({}^{n+1}\mathbf{A}_{c,\Gamma}) \tag{10} $$

which means that relation (7) is also valid for $m+1$. Therefore, invoking recurrency, expression (7) is valid for any value of m and therefore at $m = M$ which means that local and global accelerations on Γ coincide at each global time step.

Remark 2
The equality between global and local accelerations is valid for all the Newmark's time integrations schemes with $\gamma = 1/2$ [32], as the central difference scheme.

2.2. *Interface equilibrium in the reference problem*

In addition to kinematic compatibility, also equilibrium of the interface Γ should be enforced at each global time step. In order to do so, Γ is considered in what follows as a massless entity subjected to the actions transmitted by the local and complementary regions (Figure 3) and possibly to point or line loads directly applied on the interface. The equilibrium of nodes of the complementary mesh on the interface is written in term of nodal forces as follows

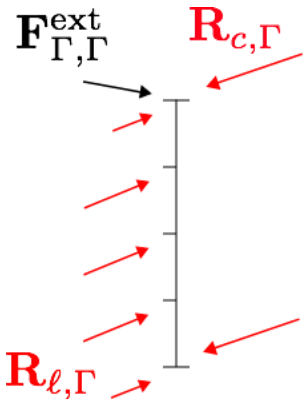

Figure 3. Free body diagram of interface between local and complementary regions in the reference problem.

$$ \Pi_h^{1T}\mathbf{R}_{\ell,\Gamma} + \mathbf{R}_{c,\Gamma} + \mathbf{F}^{\text{ext}}_{\Gamma,\Gamma} = \mathbf{0} \tag{11} $$

In (11), Π_h^{1T} is the linear spatial upscaling operator, $\mathbf{R}_{\ell,\Gamma}$ and $\mathbf{R}_{c,\Gamma}$ are the reaction forces transmitted to the interface by the local and the complementary regions, respectively (Figure 4), $\mathbf{F}^{\text{ext}}_{\Gamma,\Gamma}$ are equivalent nodal forces due to possible point or line loads directly applied on the interface. From equilibrium of the local and complementary parts, one has:

$$ \mathbf{R}_{\ell,\Gamma} = \mathbf{F}^{\text{ext}}_{\ell,\Gamma} - \mathbf{M}_{\ell,\Gamma}\mathbf{A}_{\ell,\Gamma} - \mathbf{F}^{\text{int}}_{\ell,\Gamma}, \quad \mathbf{R}_{c,\Gamma} = \mathbf{F}^{\text{ext}}_{c,\Gamma} - \mathbf{M}_{c,\Gamma}\mathbf{A}_{c,\Gamma} - \mathbf{F}^{\text{int}}_{c,\Gamma} \tag{12} $$

where $\mathbf{M}_{\ell,\Gamma}$ and $\mathbf{M}_{c,\Gamma}$ are lumped nodal masses, $\mathbf{F}^{\text{int}}_{\ell,\Gamma}$ and $\mathbf{F}^{\text{int}}_{c,\Gamma}$ are equivalent internal nodal forces and $\mathbf{F}^{\text{ext}}_{\ell,\Gamma}$ and $\mathbf{F}^{\text{ext}}_{c,\Gamma}$ are equivalent nodal forces accounting for body forces in the local and complementary regions, respectively.

DOI: 10.1002/nme

In summary, at the level of the interface Γ, the solution of the reference problem is characterized by: *a*) the compatibility of velocities at each local time step, thanks to the use of the Hermite interpolation in time (equations 1 and 2); *b*) the interface equilibrium (11), where the reaction forces at the interface, which include inertia terms, are defined by the equilibrium (12) of the local and complementary parts.

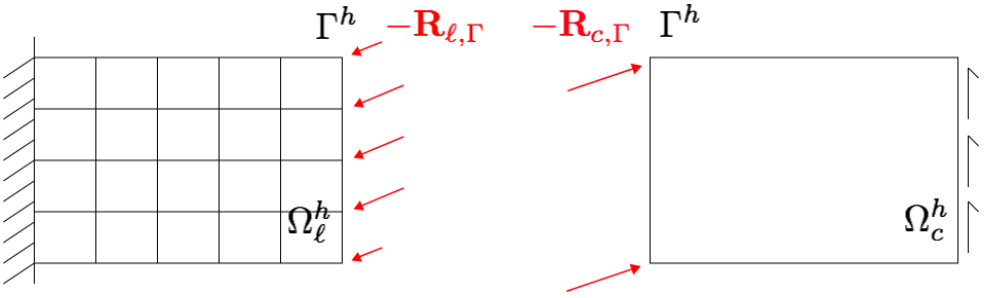

Figure 4. Reaction forces on local and complementary regions.

3. SUBSTITUTION METHOD AND MULTISCALE COMPATIBILITY CONDITION

As discussed in the introduction, heterogeneous problems can be tackled in at least two ways. A common industrial practice is to start with a global analysis (like the one in Figure 5). The problem is then re-analyzed in order to take into account non-linearities and fine structural details, or simply using a more refined mesh to assess the initial computation. This can be done either performing a complete reanalysis of the whole problem, or by making use of sub-modeling techniques, with the inherent limitations of those approaches. Another possibility, usually not available in commercial codes, is to rely on domain decomposition methods. The so called "substitution" method presented in [28] combines in a way those different approaches in a non-intrusive manner. In the case of industrial practices, what we later call the "global model" is the initial model of engineers. Let us note that it is possible to use local and global models with different assumptions as proposed in [33]. In dynamics this possibility should be associated with the use of a selective mass scaling technique as otherwise the small thickness of the structure could lead to unacceptably small time-steps [34].

The substitution method makes use of two meshes and associated time discretizations. The first mesh is the coarse global one (Figure 5), where the region of interest at the left in Figure 1 has been substituted by a coarse region, the "substitution region" (Ω^h_s in Figure 5), which usually does not contain fine geometric details and which can be furnished with a simplified material behavior. The associated problem is run only once per global time step and will be referred to as the "global problem". The second mesh concerns the "local region" of interest (Ω^h_ℓ in Figure 6). Additional nodal forces denoted by $\mathbf{P}$ have to be applied at the interface Γ^h between the complementary Ω^h_c and substitution Ω^h_s regions (Figure 5) to guarantee that the solution of the global problem is identical on the interface to the one of the reference problem. Those correction forces are intended to compensate for the different action exerted by the local region Ω^h_ℓ and by its substitution Ω^h_s on the interface Γ^h with the complementary region Ω^h_c.

The main problem in the substitution method is then the determination of the correction forces $\mathbf{P}$. Knowing those forces, the correct interface nodal velocities can be determined and applied to the local domain. If the imposed velocities on the boundary Γ are the correct ones, its response would then coincide with the one of the reference problem. In what follows, the equations to be satisfied by the correction forces $\mathbf{P}$ are derived. In Section 4, the iterative process involving only local iterations (i.e. making use of computations on the local and substitution domains only) is described.

When the local region is replaced by the substitution region and the correction forces are added on Γ, the equilibrium of the interface in the global problem in Figure 5 writes

$$\mathbf{R}_{c,\Gamma} + \mathbf{R}_{s,\Gamma} + \mathbf{P} + \mathbf{F}^{\text{ext}}_{\Gamma,\Gamma} = \mathbf{0} \tag{13}$$

DOI: 10.1002/nme

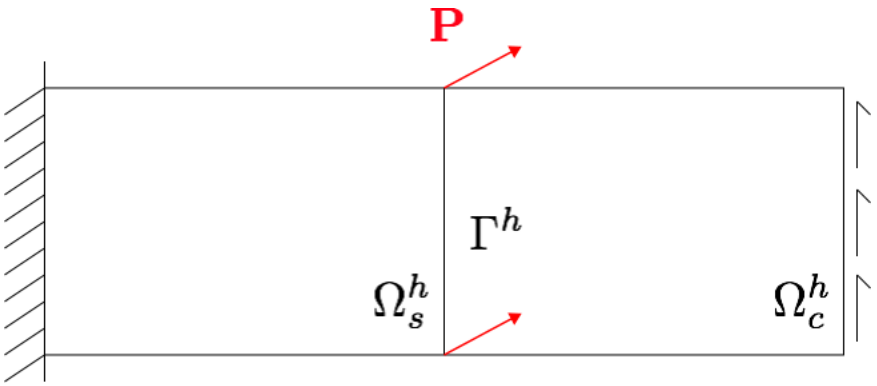

Figure 5. Discretized global problem with substitution region and correction forces $\mathbf{P}$: coarse space and time discretization.

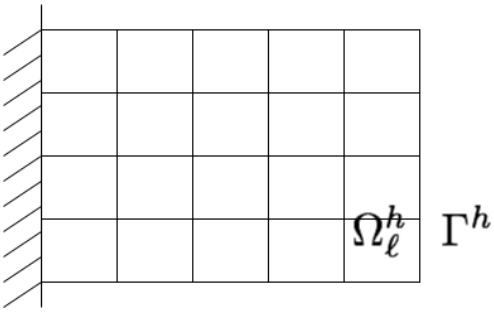

Figure 6. Local region: fine space and time discretization.

where

$$\mathbf{R}_{s,\Gamma} = \mathbf{F}^{\text{ext}}_{s,\Gamma} - \mathbf{M}_{s,\Gamma}\mathbf{A}_{s,\Gamma} - \mathbf{F}^{\text{int}}_{s,\Gamma} \tag{14}$$

The correction forces $\mathbf{P}$ are determined by imposing that the left hand sides of Equations (11) and (13) are equal at convergence:

$$\Pi_h^{1T}\mathbf{R}_{\ell,\Gamma} + \mathbf{R}_{c,\Gamma} + \mathbf{F}^{\text{ext}}_{\Gamma,\Gamma} = \mathbf{R}_{c,\Gamma} + \mathbf{R}_{s,\Gamma} + \mathbf{P} + \mathbf{F}^{\text{ext}}_{\Gamma,\Gamma} \tag{15}$$

Introducing the expressions (12) and (14) of the reactions forces, rearranging and making use of the fact that $\mathbf{A}_{c,\Gamma} = \mathbf{A}_{s,\Gamma}$ and, in view of the acceleration compatibility property in (7), i.e., $\mathbf{A}_{\ell,\Gamma} = \Pi_h^1\mathbf{A}_{c,\Gamma}$ at the beginning and the end of each global time step, one obtains the following multiscale compatibility condition, which establishes the connection between the global and local problems at different scales, consistent with the assumed definition of the reference problem

$$\left(\Pi_h^{1T}\mathbf{M}_{\ell,\Gamma}\Pi_h^1 - \mathbf{M}_{s,\Gamma}\right)\mathbf{A}_{s,\Gamma} + \left(\Pi_h^{1T}\mathbf{F}^{\text{int}}_{\ell,\Gamma} - \mathbf{F}^{\text{int}}_{s,\Gamma}\right) + \mathbf{P} - \left(\Pi_h^{1T}\mathbf{F}^{\text{ext}}_{\ell,\Gamma} - \mathbf{F}^{\text{ext}}_{s,\Gamma}\right) = \mathbf{0} \tag{16}$$

Equations (13) and (16), enforced at the end of each time step, will be used in Section 4 to formulate the iterative scheme for the computation of the correction forces $\mathbf{P}$.

4. ITERATIVE SUBSTITUTION ALGORITHM

The proposed multiscale iterative method is intended to search for a solution of the reference problem defined in Section 2, in the considered global time step $\Delta t_c = t^{n+1} - t^n$, by means of a solution of the global problem, to be carried out only once, and of an iterative solution of the local problem. The procedure is constructed in two phases.

DOI: 10.1002/nme

- Pre-computation phase. The global problem is solved using the coarse macroscopic space and time discretization everywhere. Other terms involving data transmitted from the lower scale are computed only once using information available from the previous time step.
- Correction phase. New estimates of the correction forces ${}^{n+1}\mathbf{P}$ on the interface Γ are computed by repeated solutions of the local problem, involving the fine space and time discretization.

To simplify the presentation, the problem is formulated in incremental form, where incremental quantities $\Delta\square = {}^{n+1}\square - {}^{n}\square$ are defined over the considered global time step.

Assume that the solution of the global and local problems, including the correction forces ${}^{n}\mathbf{P}$, is completely known at $t = t^n$, and that increments of external forces $\Delta\mathbf{F}^{\text{ext}}_{c,\Gamma}$ and $\Delta\mathbf{F}^{\text{ext}}_{\ell,\Gamma}$ and possibly $\Delta\mathbf{F}^{\text{ext}}_{\Gamma,\Gamma}$ are assigned. The global interface equilibrium equation (13) and the multiscale compatibility condition (16) in incremental form read

$$\begin{aligned}
\left(\mathbf{M}_{c,\Gamma} + \mathbf{M}_{s,\Gamma}\right)\Delta\mathbf{A}_{s,\Gamma} + \left(\Delta\mathbf{F}^{\text{int}}_{s,\Gamma} + \Delta\mathbf{F}^{\text{int}}_{c,\Gamma}\right) &= \Delta\mathbf{P} + \Delta\mathbf{F}^{\text{ext}}_{s,\Gamma} + \Delta\mathbf{F}^{\text{ext}}_{c,\Gamma} + \Delta\mathbf{F}^{\text{ext}}_{\Gamma,\Gamma} \\
\left(\Pi^{1T}_h\mathbf{M}_{\ell,\Gamma}\Pi^{1}_h - \mathbf{M}_{s,\Gamma}\right)\Delta\mathbf{A}_{s,\Gamma} + \left(\Pi^{1T}_h\Delta\mathbf{F}^{\text{int}}_{\ell,\Gamma} - \Delta\mathbf{F}^{\text{int}}_{s,\Gamma}\right) &= -\Delta\mathbf{P} + \left(\Pi^{1T}_h\Delta\mathbf{F}^{\text{ext}}_{\ell,\Gamma} - \Delta\mathbf{F}^{\text{ext}}_{s,\Gamma}\right)
\end{aligned} \tag{17}$$

Summing up the two equations (17), one can eliminate $\Delta\mathbf{P}$, obtaining

$$\left(\Pi^{1T}_h\mathbf{M}_{\ell,\Gamma}\Pi^{1}_h + \mathbf{M}_{c,\Gamma}\right)\Delta\mathbf{A}_{s,\Gamma} + \left(\Pi^{1T}_h\Delta\mathbf{F}^{\text{int}}_{\ell,\Gamma} + \Delta\mathbf{F}^{\text{int}}_{c,\Gamma}\right) = \Pi^{1T}_h\Delta\mathbf{F}^{\text{ext}}_{\ell,\Gamma} + \Delta\mathbf{F}^{\text{ext}}_{c,\Gamma} + \Delta\mathbf{F}^{\text{ext}}_{\Gamma,\Gamma} \tag{18}$$

Some of the terms in (18) can be computed only once per global time step, using information coming from the solution of the global problem or from the previous time step, while others have to be computed iteratively. Terms of the first type are used to define pre-computation values $\Delta\mathbf{A}^{\text{prec}}_{s,\Gamma}$ of the acceleration increment, while terms of the second type provide iterative corrections $\Delta\mathbf{A}^{\text{corr}}_{s,\Gamma}$:

$$\begin{aligned}
\Delta\mathbf{A}^{\text{prec}}_{s,\Gamma} &= \left(\Pi^{1T}_h\mathbf{M}_{\ell,\Gamma}\Pi^{1}_h + \mathbf{M}_{c,\Gamma}\right)^{-1}\left[\Pi^{1T}_h\,{}^{n}\mathbf{F}^{\text{int}}_{\ell,\Gamma} - \Delta\mathbf{F}^{\text{int}}_{c,\Gamma} + \left(\Pi^{1T}_h\Delta\mathbf{F}^{\text{ext}}_{\ell,\Gamma} + \Delta\mathbf{F}^{\text{ext}}_{c,\Gamma} + \Delta\mathbf{F}^{\text{ext}}_{\Gamma,\Gamma}\right)\right] \\
\left(\Delta\mathbf{A}^{\text{corr}}_{s,\Gamma}\right)^{i+1} &= \left(\Pi^{1T}_h\mathbf{M}_{\ell,\Gamma}\Pi^{1}_h + \mathbf{M}_{c,\Gamma}\right)^{-1}\left[-\Pi^{1T}_h\left({}^{n+1}\mathbf{F}^{\text{int}}_{\ell,\Gamma}\right)^{i}\right]
\end{aligned} \tag{19}$$

In $(19)_1$, $\Pi^{1T}_h\,{}^{n}\mathbf{F}^{\text{int}}_{\ell,\Gamma}$ is known from the previous step, $\Delta\mathbf{F}^{\text{int}}_{c,\Gamma}$ is also known from the previous step, since in the central difference scheme nodal displacements are an outcome of the explicit integration and are computed directly from the known accelerations. In $(19)_2$, $\Pi^{1T}_h\left({}^{n+1}\mathbf{F}^{\text{int}}_{\ell,\Gamma}\right)^{i}$ are the updated internal forces of the local problem on the interface Γ, computed on the basis of the current estimate of acceleration increments $\Delta\mathbf{A}^{\text{prec}}_{s,\Gamma} + \left(\Delta\mathbf{A}^{\text{corr}}_{s,\Gamma}\right)^{i}$. At the end of the pre-computation phase, the local internal forces are initialized assigning on the interface the pre-computation value $\Delta\mathbf{A}^{\text{prec}}_{s,\Gamma}$ only.

The iterative procedure is stopped when an assigned tolerance $\bar{e}$ on the error on interface equilibrium at the global level is met. The used error measure is defined as follows

$$e = \frac{\|\mathbf{R}_{c,\Gamma} + \Pi^{1T}_h\mathbf{R}_{\ell,\Gamma} + \mathbf{F}^{\text{ext}}_{\Gamma,\Gamma}\|_{L^2(\Gamma)}}{\|\mathbf{F}^{\text{ext}}\|_{L^2(\partial\Omega)}} \tag{20}$$

Compared to the direct solution of the reference problem, the proposed iterative multiscale approach implies at each time step the solution of the global problem, which however has been discretized by means of a coarse mesh and possibly with a simplified geometry and material behavior. It is therefore expected to be significantly less expensive than the original problem. On the other hand, the local problem, requires an accurate description of geometry and material behavior and a fine mesh, but concerns a small part of the problem domain, so that its iterative solution can be carried out with little computational effort. Once a converged estimate of $\Delta\mathbf{A}^{\text{corr}}_{s,\Gamma}$ has been achieved, the correction forces to be used for the next time step are updated using Equation $(17)_2$:

$$\begin{aligned}
{}^{n+1}\mathbf{P} = {}^{n}\mathbf{P} + \Delta\mathbf{P} = {}^{n}\mathbf{P} &- \left(\Pi^{1T}_h\mathbf{M}_{\ell,\Gamma}\Pi^{1}_h + \mathbf{M}_{c,\Gamma}\right)\left(\Delta\mathbf{A}^{\text{prec}}_{s,\Gamma} + \Delta\mathbf{A}^{\text{corr}}_{s,\Gamma}\right) \\
&- \left(\Pi^{1T}_h\Delta\mathbf{F}^{\text{int}}_{\ell,\Gamma} + \Delta\mathbf{F}^{\text{int}}_{c,\Gamma}\right) + \left(\Pi^{1T}_h\Delta\mathbf{F}^{\text{ext}}_{\ell,\Gamma} - \Delta\mathbf{F}^{\text{ext}}_{s,\Gamma}\right)
\end{aligned} \tag{21}$$

DOI: 10.1002/nme

5. APPLICATIONS

The performance of the method described in the paper is illustrated by means of three examples: *i*) local region consisting of a mesh refinement of the substituted region; *ii*) local region with heterogeneities of various types; *iii*) model adaptation in the case of delamination propagation. In all cases, the results are compared with the first version of the substitution method presented in [28], where the case of mesh refinement was treated and compared in detail with different domain decomposition algorithms [18, 35, 36]. The same type of examples is used here to comparatively assess the convergence property of the method described in this paper with respect to the one presented in [28]. The example with heterogeneities is used to show the robustness of the proposed method both in terms of quality of results when compared to a domain decomposition method and of convergence rate. The last example is a first attempt to apply the method to a more complex case involving non-linearities and model adaptation. In all cases, the tolerance criteria for the error (20) is set at $\overline{e} = 1\%$. In fact, it was shown in [28] that with such a tolerance the results obtained in terms of velocity match nearly perfectly those obtained by a domain decomposition approach.

5.1. Local region with mesh refinement

The elastic global model of the structure is discretized by a coarse mesh of two 4-node quadrilateral bilinear displacement-based finite elements. The local model consists of a refined mesh made of smaller finite elements of the same type (as in Figure 7) concerning only a limited region of the structure, close to the fixed boundary, in order to attenuate the locking effects. The data of the problem are the following: density $\rho = 7800$ kg/m^3; Young's modulus $E = 210 \cdot 10^9$ Pa; Poisson's ratio $\nu = 0.3$; length $L = 30$ m; height $H = 10$ m. A uniform and constant in time shear load $\overline{f} = 3 \cdot 10^6$ N/m^2 is applied on the right side of the structure.

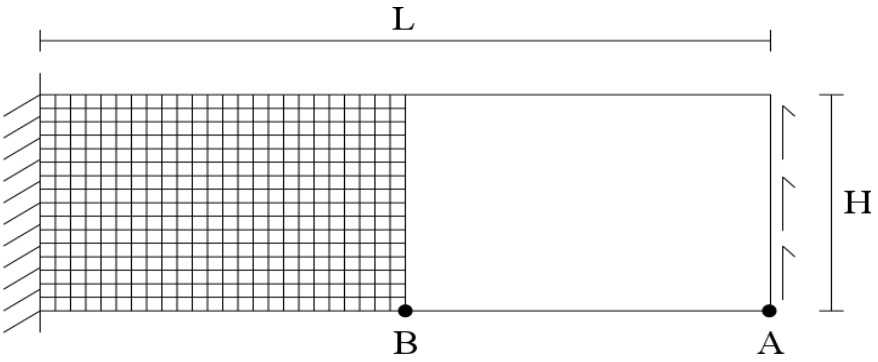

Figure 7. Spatial discretization and monitored points A and B.

The time steps at the two scales are chosen in accordance with the estimation of the critical time step at the local and global levels, so that:

- $\Delta t_c = 0.8 \cdot 10^{-3}$ s in the global analysis;
- $\Delta t_\ell = \Delta t_c / h = 0.05 \cdot 10^{-3}$ s in the local analysis;

where $h = 16$ is the global/local mesh size ratio.

Figure 8 shows time histories of accelerations at points A and B, obtained with the original and enhanced substitution methods. It can be observed that curves corresponding to the same location are virtually identical.

In Figure 9a, the number of iterations needed to achieve convergence with the original algorithm [28] (dashed line) and the enhanced one (solid line) are compared. The number of iterations required for a given tolerance in the original algorithm ranged between 3 and 9 (maximum of 8 in this example) for all the tests that were carried out, while the range has always been between 1 and 3 for the enhanced algorithm. Therefore, no other results of this type will be displayed for the other examples. For the example treated in this paragraph, the "periodic" pattern of the number

DOI: 10.1002/nme

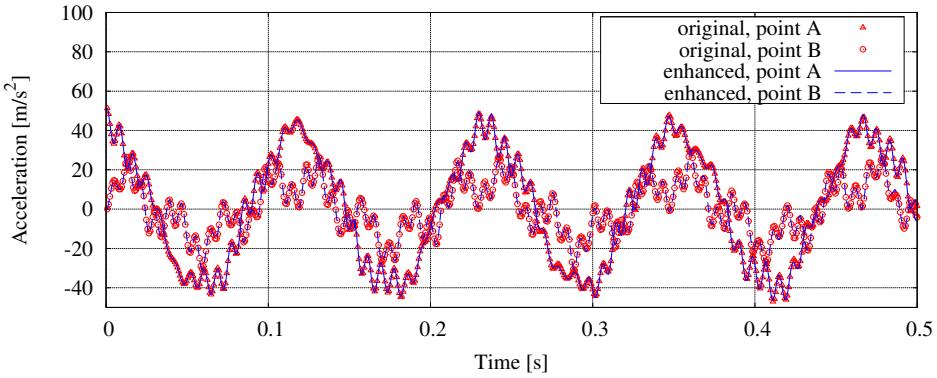

Figure 8. Vertical accelerations at points A and B for original and enhanced substitution methods.

of iterations is explained by the "oscillatory" response of the structure which can be observed in Figure 9b, where the displacement history at point B is superposed to the plot of the number of iterations per time step. The number of required iterations is greater when the displacement is larger.

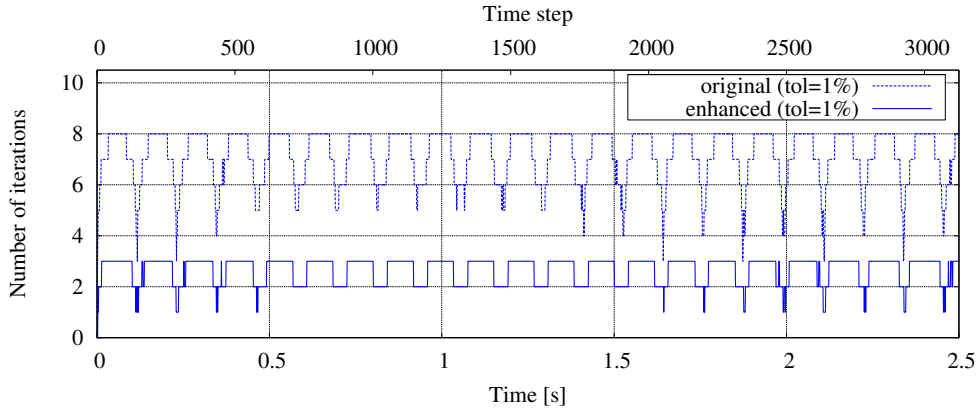

(a) *Number of iterations to convergence per time step in original and enhanced algorithms.*

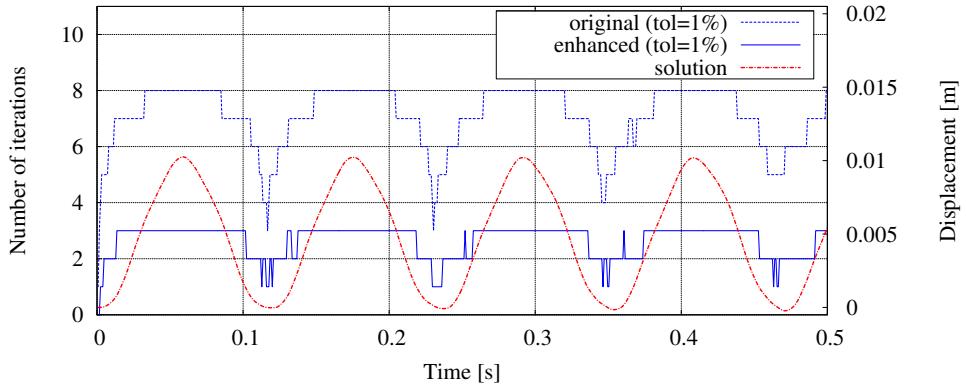

(b) *Displacement evolution at point B and corresponding number of iterations.*

Figure 9. Assessment of convergence property.

The fast convergence of the enhanced algorithm can be better appreciated in Figure 10, where convergence of vertical acceleration of point B is shown over a short period of time. The blue line represents the solution at convergence, while the square markers denote the solution in the

DOI: 10.1002/nme

pre-computation phase (iteration 0), which does not take into account the local internal forces. The improvement of precision after the first iteration is noticed by looking at the circular markers, which are already very close to the converged solution.

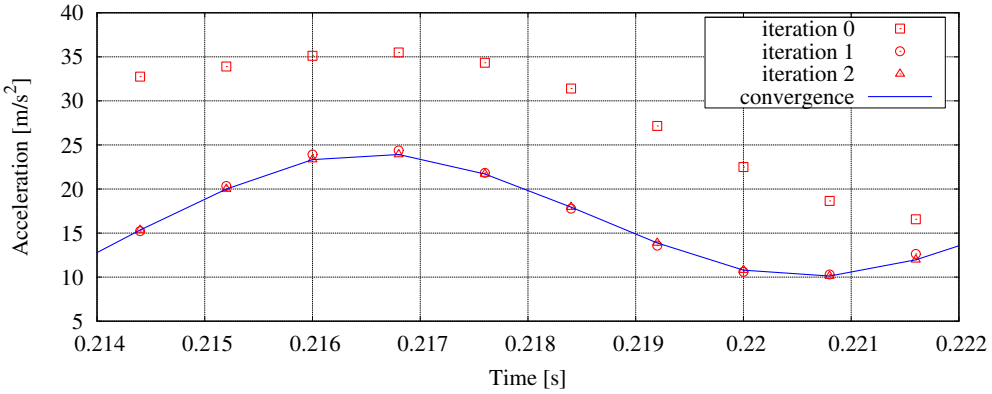

Figure 10. Enhanced approach: evolution with iterations of vertical acceleration at point B.

Figure 11 allows to compare the rate of convergence of the two algorithms at different time instants. at all the considered times, the enhanced method exhibits a higher convergence rate, which does not change along the history of deformation.

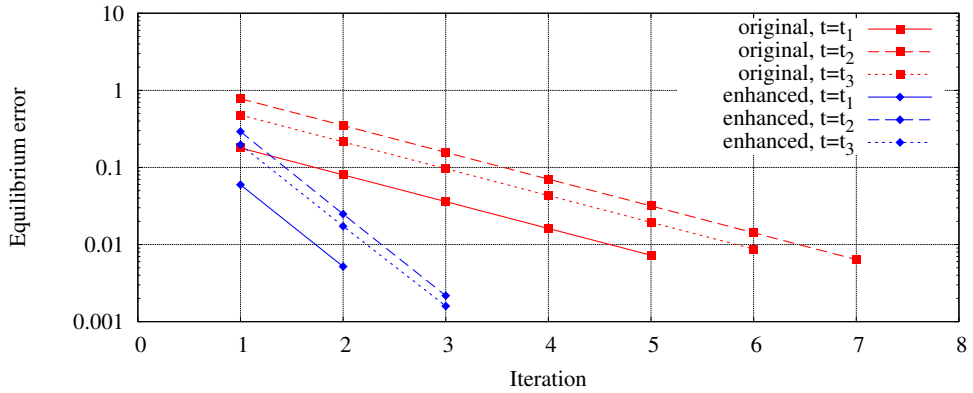

Figure 11. Convergence rate of original [28] and enhanced methods at three time instants: $t_i = \frac{1+i}{6} t_{\text{end}}$ with $i = 1, 2, 3$ and $t_{\text{end}} = 2.5$ s.

5.2. *Local region with heterogeneities*

One of the potential uses of the substitution algorithm concerns the computation of a structure with a part which is characterized by small features. To study this type of situation, we consider the introduction of heterogeneities (either holes or stiff inclusions) in the previous model, as shown in Figure 12, where point S, which will be subsequently used in the presentation of the results, has been singled out. The substitution method allows to use the same homogeneous global model used in the previous case, the heterogeneities being introduced at the local level only.

The introduction of holes does not modify the critical time step of the local model. This is not the case when introducing stiff inclusions, which have been assumed to have a density equal to the density of the surrounding material and a ten times larger Young's modulus. For stiff inclusions, this leads to a local time step equal to: $\Delta t_\ell = \Delta t_c / \tilde{h} = 0.0333 \cdot 10^{-3}$ s.

The presence of heterogenities, either holes or stiff inclusions, does not affect the convergence rate, as can be seen in Figure 13. The only minor difference with respect to the homogeneous case

DOI: 10.1002/nme

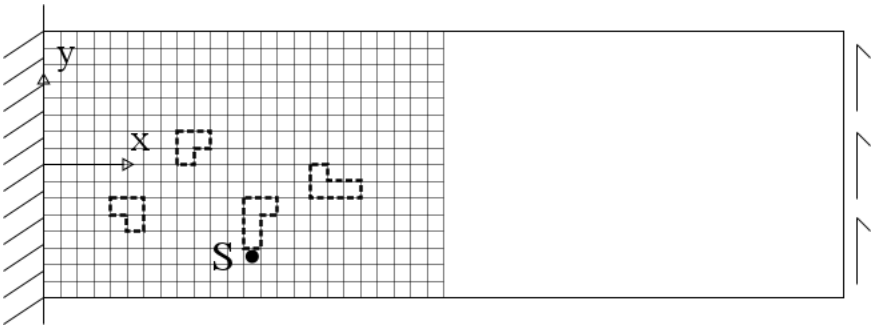

Figure 12. Local region with heterogeneities. Definition of point S at which solution is monitored.

concerns the initial error which is larger as the used global model is less representative of the real structural behavior.

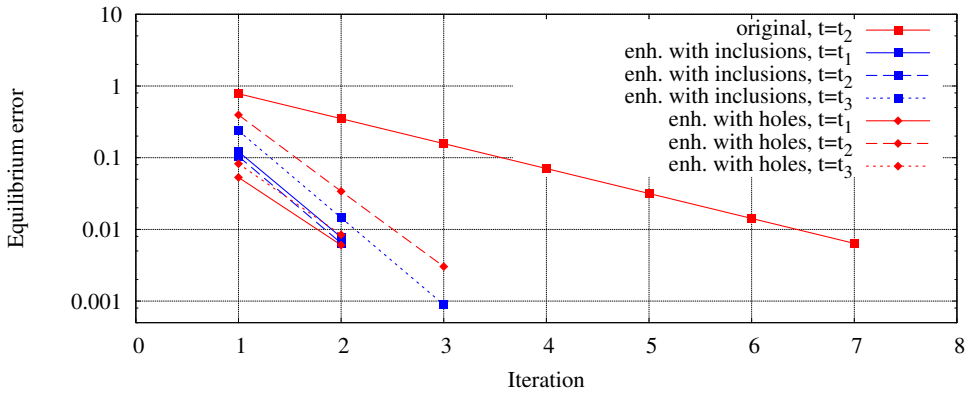

Figure 13. Local region with heterogeneities. Convergence rate at three time instants $t_i = \frac{1+i}{6} t_{\text{end}}$ ($i = 1, 2, 3$ and $t_{\text{end}} = 2.5$ s), compared to convergence rate of homogeneous problem solved with original method [28].

Figure 14 shows the numerical results in terms of velocity time histories at point B in Figure 7, for the case with holes. The solid blue line is the solution obtained with the proposed algorithm while the red circles denote the solution obtained with the domain decomposition method [18]. The same agreement is found in the case of stiff inclusions.

Let $\overline{\sigma}_x$ denote the horizontal stress at point S in the static solution of the homogeneous problem (i.e. without holes or inclusions), for an applied shear load equal to its final constant value. Figures 15(a), for the case with holes, and 15(b), for the case with rigid inclusions, show contours of the normalized stress $\sigma_x/\overline{\sigma}_x$ at point S at the instants when it attains its maximum value in the two cases. In Figure 15(c), the histories of $\sigma_x/\overline{\sigma}_x$ at point S are compared with the one obtained without heterogeneities. The expected effects of both holes and inclusions are confirmed in all cases.

5.3. Application to a composite structure with damageable interface

A detailed study of structural response up to failure often requires taking into account phenomena which spread over multiple spatial and temporal scales. A potential application of the substitution method is to treat this type of problems by introducing local space/time refinements only when and where needed, avoiding complex implementation issues. In this subsection, as a first and highly simplified test, the adaptive introduction of an evolving local region has been considered for the dynamic simulation of delamination in an End Loaded Split test, as described in Figure 16, using a damage mechanics approach. A test of this type is of potential interest for Airbus [37]. The structure, composed of two linear elastic plies connected by a damageable cohesive interface, is of length

DOI: 10.1002/nme

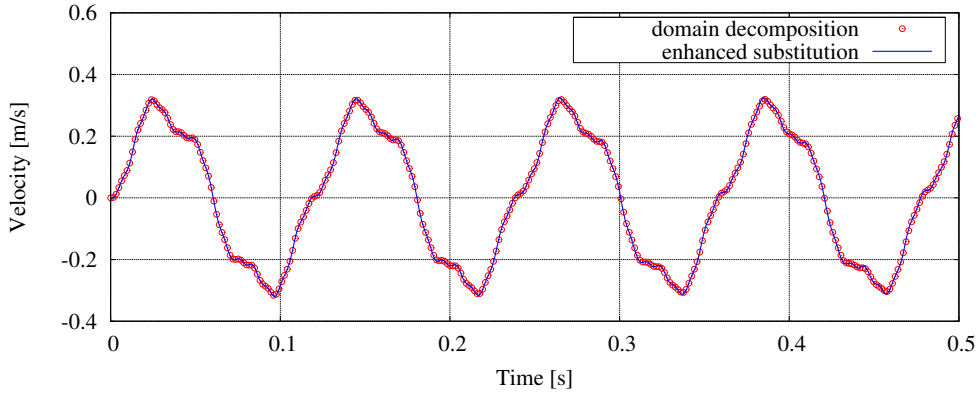

Figure 14. Vertical velocities at the point B of Figure 7, obtained with domain decomposition and enhanced methods.

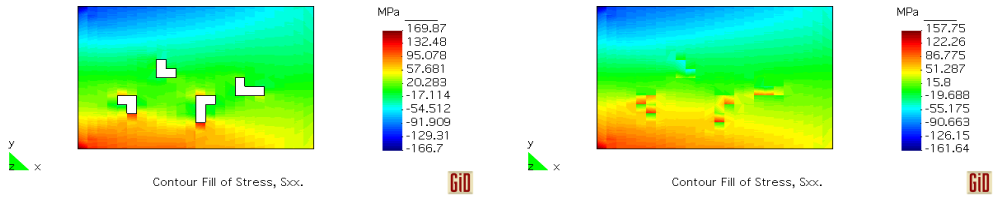

(a) *Stress σ_x over the local domain at the time instant $t = 0.0616$ s.*

(b) *Stress σ_x over the local domain at the time instant $t = 0.0592$ s.*

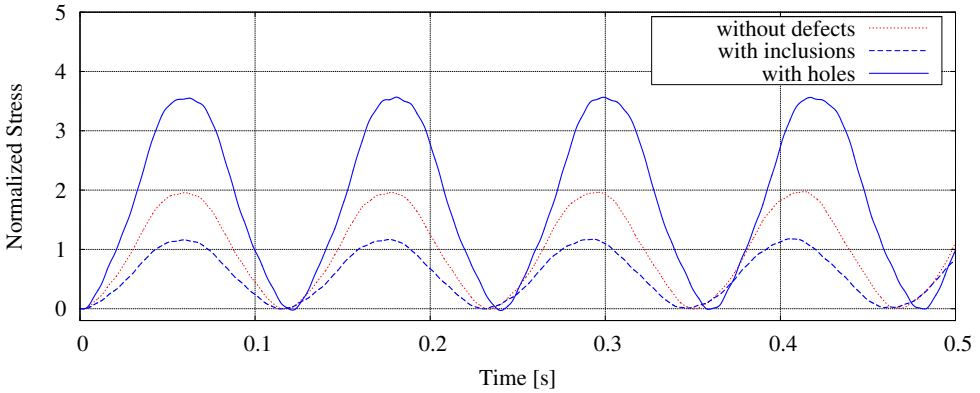

(c) *Stress histories $\sigma_x(t)$ at the point S normalized by the static estimation $\overline{\sigma}_x$*

Figure 15. Effect of heterogeneities on the axial stress distribution.

$L = 1$ m and of height $H = 0.1$ m and is subjected to a constant concentrated tip load $\overline{f} = 10^7$ N/m. The load is applied at the top right corner of the beam, as shown in Figure 16, to reproduce a loading condition of the type encountered in impact problems.

The damage evolution law used in the cohesive interface writes:

$$\dot{d} = \frac{1}{\tau_c}\left(1 - \mathrm{e}^{-<\frac{1}{2}\frac{\overline{Y}-Y_0}{Y_c-Y_0}-d>_+}\right) \tag{22}$$

where τ_c is the characteristic time of the fracture process, $< \square >_+$ denotes the positive part of the quantity $\square$, Y_0 and Y_c are the threshold and critical thermodynamical forces, respectively, and $\overline{Y}$ is

DOI: 10.1002/nme

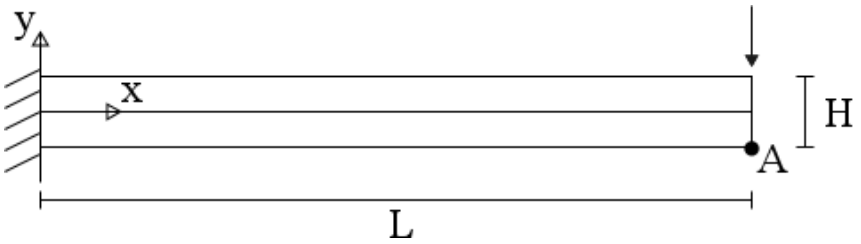

Figure 16. *End Loaded Split* (*ELS*) test case: monitored point A and coordinates system.

defined as:

$$\overline{Y} = \sup_{\tau \leq t} Y(t)|_\tau \quad \text{with} \quad Y(t) = \frac{1}{2}\left(\frac{< \sigma_n >_+^2}{k_0(1-d)^2} + \frac{\sigma_{nt}^2}{k_0(1-d)^2} \right) \tag{23}$$

where k_0 is the cohesive interface stiffness, σ is the stress in the cohesive interface and n and t denote the directions normal and tangential to the cohesive interface. The damage variable d is bounded between the values 0, in which case the cohesive interface is not damaged, and 1, in which case the cohesive interface is completely damaged.

The problem data are as follows. For the linear elastic plies: $\rho = 1500$ kg/m^3; $E = 140 \cdot 10^9$ Pa; $\nu = 0.4$. For the cohesive interface: $\tau_c = 20 \cdot 10^{-5}$ s; $Y_0 = 50 \cdot 10^3$ Pa; $Y_c = 230 \cdot 10^3$ Pa; $k_0 = 10^{12}$ N/m^3. The adopted high value of k_0 is intended to penalize possible interpenetration between the plies.

The substitution method couples here a coarse global analysis of the whole structure with an adaptive refined analysis of a local region that progressively increases its size to follow the delamination propagation (see Figure 17). While the global coarse mesh remains the same throughout the analysis, the interface between the complementary and the local regions moves to the left as the analysis progresses.

The global coarse model $\Omega_g^{h,\text{eas}} \equiv \Omega_c^h \cup \Omega_s^h$ is made of 4-node *EAS-7* quadrilateral elements (of the type introduced in [38], following [39] and [40]), featuring a constant shear stress σ_{xy} and a normal stress $\sigma_x(x, y)$, constant along x and linearly varying along y, with 2×2 Gauss points. The local adaptive model is composed by an assembly of elementary local units, each one composed by 4×4 displacement-based quadrilateral elements and four cohesive elements placed along the interface between elements above and below the block horizontal middle line. A new unit is added to the left side of the local region each time that its interface Γ^h with the complementary region moves to the left. The local problem is solved by making use of the domain decomposition method proposed in [18], where each elementary local unit is treated as a subdomain of the local region. The global time step is $\Delta t_c = 2 \cdot 10^{-6}$ s and the local one is $\Delta t_\ell = \Delta t_c / h = 0.5 \cdot 10^{-6}$ s.

The interface Γ^h, separating the substitution and the complementary regions, is defined by the red nodes in Figure 17. In this case, as a reference solution we consider the one obtained by applying the domain decomposition method to the structure entirely discretized by local units since the beginning of the analysis. Since all the subdomains have in this case the same spatial and temporal discretization, this solution coincides with the one which would be obtained by a monolithic approach.

The adaptive definition of the local region is governed by a simple activation criterion in the global analysis. A new local unit is activated when $\mid \sigma_x^{\text{sup}} - \sigma_x^{\text{inf}} \mid /2 > \bar{\sigma}$, where σ_x^{sup} is the σ_x stress component at the two Gauss points above the cohesive interface (in the EAS7 elements σ_x is linear along y but constant along x), while σ_x^{inf} is the corresponding value in the Gauss points below the interface. The threshold $\bar{\sigma}$ has to be tuned in such a way that the cohesive process zone is entirely contained within the local region. In the considered example, the interface parameters are such that the process zone extends over the length of several units, so that new units have to be introduced very early. Three different threshold values have been tested for $\bar{\sigma}$: $\bar{\sigma} = 100 \times 10^6$ Pa, $\bar{\sigma} = 300 \times 10^6$ Pa, $\bar{\sigma} = 500 \times 10^6$ Pa. These will be denoted in the figures as "act1", "act2" and "act3", respectively.

DOI: 10.1002/nme

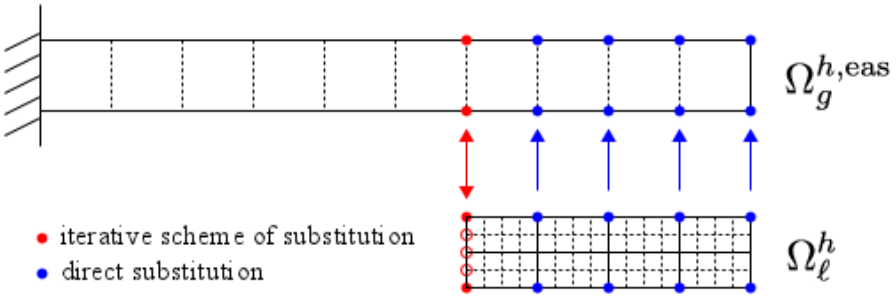

Figure 17. ELS test case: substitution strategy.

For example, Figure 18 shows the numerical results in terms of the vertical velocity of point A. The dashed red line denotes the reference solution. The blue lines indicate the solution with the adaptive substitution method: the dashed and solid lines have respectively the activation value $\overline{\sigma} = 500 \cdot 10^6$ Pa (delayed activation) and $\overline{\sigma} = 100 \cdot 10^6$ Pa (early activation). As it can be seen from the plot, the particular type of loading, inducing normal stresses in the interface between the plies, activates the structure highest eigenfrequencies due to the high value of the interface stiffness k_0. This aspect is emphasized in the curves relevant to the substitution method, due to reflections produced by the interface between the local and complementary regions. The same type of spurious high frequency oscillations would have been obtained with any other domain decomposition method with non-matching meshes.

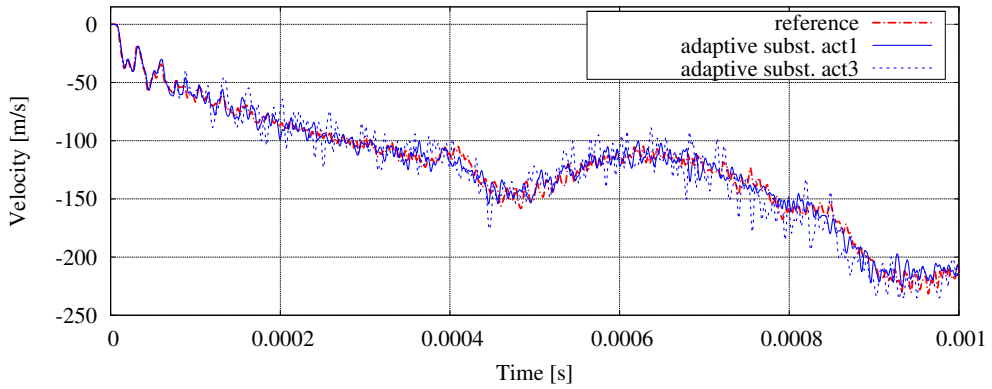

Figure 18. ELS test case: vertical velocity at point A using monolithic refined analysis (reference, red dashed curve) and adaptive substitution method, with two different activation thresholds (blue solid and dashed curves).

The predicted position of the delamination front also strongly depends on the adopted activation criterion, as can be seen in Figure 19, where three different delamination fronts, obtained using the three different activation thresholds, are compared: the dashed line corresponds to an activation threshold $\overline{\sigma} = 500 \cdot 10^6$ Pa, the short-dashed line to $\overline{\sigma} = 300 \cdot 10^6$ Pa and the dotted line to $\overline{\sigma} = 100 \cdot 10^6$ Pa. In all cases, the cohesive process zone is always entirely contained in the local region.

Figure 20 shows a sequence of snapshots of the analysis. Starting from a local region discretized by means of two units at $t = 0$ s, it progressively increases its size in order to include the delamination front and process zone tip, arriving at a final size of nine subdomains at $t_{\text{end}} = 0.001$ s.

Figure 21 shows the convergence rate at three representative time instants. As it can be observed, this is comparable to the one obtained in the previous example for a purely elastic material behavior. However, in this case the initial error is higher. This is due to the fact that the error associated to the global coarse model is higher than in the previous examples.

DOI: 10.1002/nme

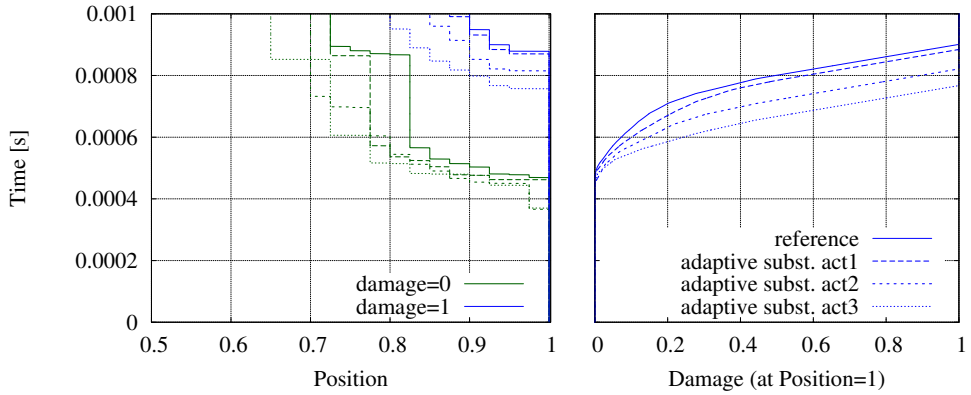

Figure 19. ELS test case: delamination process zone and damage evolution for different activation thresholds for local region expansion.

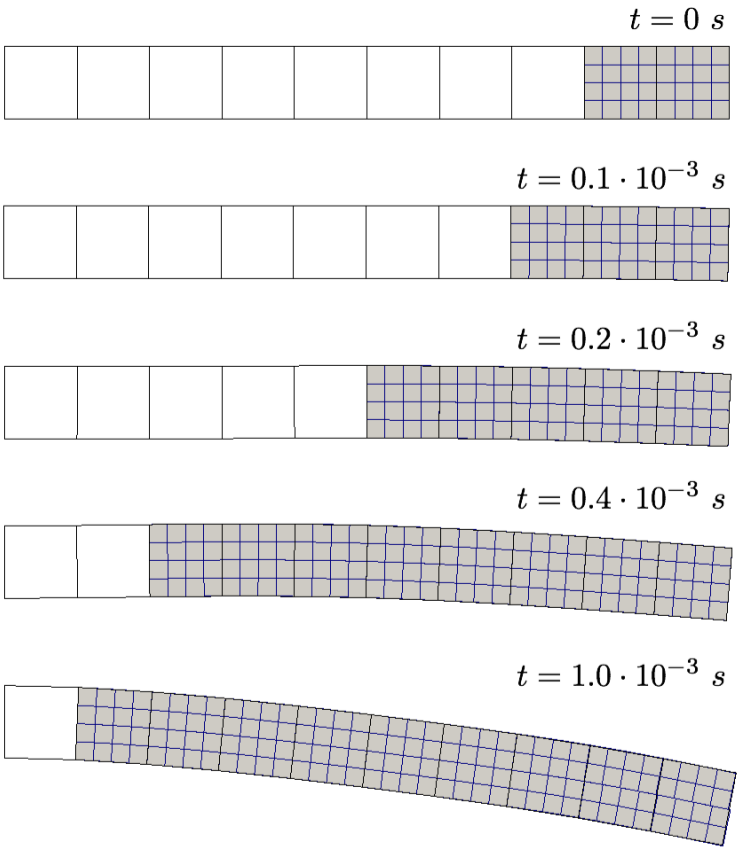

Figure 20. ELS test case: analysis snapshots at five representative time instants for $\bar{\sigma} = 500$ Pa (act3).

The previous example deserves several comments. First, the elements used for the global model are quite different from the ones used in the local region as, for example, their stiffness does not coincide with the condensed stiffness of the underlying local model. This probably amplifies the issue of spurious reflections at the interface between the two models. Moreover, in the present nonlinear dynamics context, the prediction of damages on the basis of the value of local quantities and nonlinearity governed by local quantities, such as interface stresses, raises the question of the precision of these local quantities, a question which should be addressed in future work. The use of

DOI: 10.1002/nme

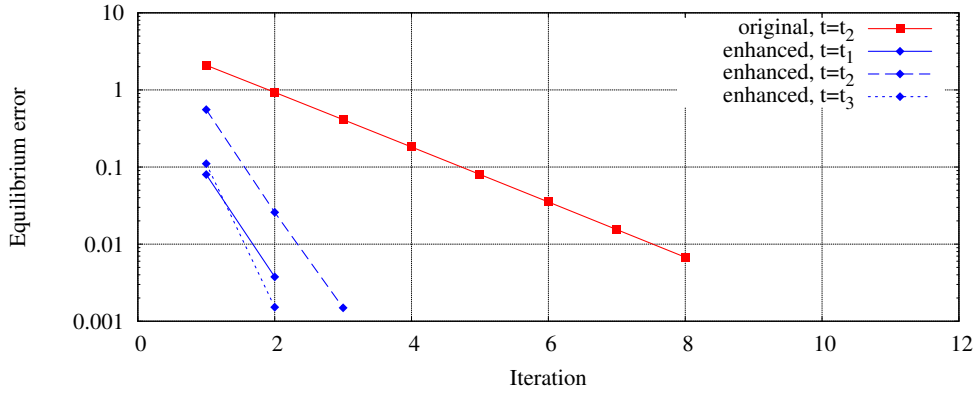

Figure 21. ELS test case. Convergence rate at three time instants $t_i = \frac{1+i}{6} t_{\text{end}}$ $(i = 1, 2, 3$ and $t_{\text{end}} = 0.001$ s) in the *ELS* test case.

adapted interfaces, avoiding spurious high frequency reflections, is in any case a subject of interest in all multiscale and domain decomposition approaches in dynamics (see, e.g., [41]).

6. CONCLUSIONS

The primary goal of this study was to improve the convergence performance of the substitution method proposed in [28]. This has been achieved thanks to the compatibility, shown in the paper, between the central difference scheme and the Hermite interpolation used as a down-scaling time operator. Based on this property, a consistent interface mass matrix has been derived which allows to reduce the number of iterations to a level which is now considered as acceptable for applications of practical interest.

The last example, concerning a delamination problem, has shown the potential applicability of the approach to nonlinear problems and opens the way to interesting future developments. A useful enhancement would consist, e.g., of the possibility to have a moving local region, placed around the current process zone, while the rest of the structure remains discretized by a coarse mesh. Unlike in the present example, where the local region can only increase its size, this would mean that regions that at certain point belonged to the local region, could return to a coarse discretization with a weakened constitutive behavior if a suitable indicator signals that there is no more need for a fine discretization, in the line of what proposed, e.g. in [42, 43, 44], where a crack was embedded on top of a given finite element model.

A pilot implementation of the method in Abaqus/Explicit is in progress, though currently is restricted to simple truss models (upcoming work should eliminate these limitations). The consideration of more complex models is of course mandatory to be able to test the feasibility of the method in problems of industrial interest. Current work also concerns the theoretical determination of the rate of convergence of the substitution method both in static and dynamics.

REFERENCES

1. Farhat C, Mandel J. The two-level FETI method for static and dynamic plate problems Part I: An optimal iterative solver for biharmonic systems. *Computer Methods in Applied Mechanics and Engineering* 1998; **155**(1-2):129–151.
2. Rixen D, Farhat C, Géradin M. A two-step hybrid method for the static and dynamic analysis of substructure problems with conforming and non-conforming interfaces. *Computer Method in Applied Mechanics and Mathematics* 1998; **154**:229–264.
3. Ladevèze P, Dureisseix D. A 2-level and mixed domain decomposition approach for structural analysis. *Contemporary mathematics* 1998; :246–253.

DOI: 10.1002/nme

4. Gosselet P, Rey C. Non-overlapping domain decomposition methods in structural mechanics. *Archives of Computational Methods in Engineering* 2006; **13**:515–572.
5. Cresta P, Allix O, Rey C, Guinard S. Nonlinear localization strategies for domain decomposition methods: Application to post-buckling analyses. *Computer Methods in Applied Mechanics and Engineering* 2007; **196**:1436–1446.
6. Ladevèze P, Loiseau O, Dureisseix D. A micro–macro and parallel computational strategy for highly heterogeneous structures. *International Journal for Numerical Methods in Engineering* 2001; **52**:121–138.
7. Ladevèze P, Passieux JC, Neron D. The latin multiscale computational method and the proper generalized decomposition. *Computer Methods in Applied Mechanics and Engineering* 2010; **199**(21-22):1287–1296.
8. Allix O. A composite damage meso-model for impact problems. *Composites Science and Technology* 2001; **61**:2193–2205.
9. Germain N, Besson J, Feyel F, Gosselet P. High-performance parallel simulation of structure degradation using non-local damage models. *International Journal for Numerical Methods in Engineering* 2007; **71**:253–276.
10. Kerfriden P, Allix O, Gosselet P. A three-scale domain decomposition method for the 3D analysis of debonding in laminates. *Computational Mechanics* 2009; **44**(3):343–362.
11. Allix O, Kerfriden P, Gosselet P. A relocalization technique for the multiscale computation of delamination in composite structures. *Computer Modeling in Engineering and Sciences* 2010; **55**(3):271–292.
12. Allix O, Kerfriden P, Gosselet P. On the control of the load increments for a proper description of multiple delamination in a domain decomposition framework. *International Journal for Numerical Methods in Engineering* 2010; **83**:1518–1540.
13. Saavedra K, Allix O, Gosselet P. On a multiscale strategy and its optimization for the simulation of combined delamination and buckling. *International Journal for Numerical Methods in Engineering* 2012; **91**(7):772–798.
14. Belytschko T, Mullen R. Stability of explicit-implicit mesh partitions in time integration. *International Journal for Numerical Methods in Engineering* 1978; **12**:1575–1586.
15. Hughes TJR, Liu WK. Implicit-explicit finite element in transient analysis: stability theory. *Journal of Applied Mechanics* 1978; **45**:371–374.
16. Smolinski P, Belytschko T, Neal M. Multi-time-step integration using nodal partitioning. *International Journal for Numerical Methods in Engineering* 1988; **26**:349–359.
17. Daniel WJT. A partial velocity approach to subcycling structural dynamics. *Computer Methods in Applied Mechanics and Engineering* 2003; **192**(3):375–394.
18. Gravouil A, Combescure A. Multi-time-step explicit-implicit method for non-linear structural dynamics. *International Journal for Numerical Methods in Engineering* 2001; **50**:199–225.
19. Combescure A, Gravouil A. A numerical scheme to couple subdomains with different time-steps for predominantely transient linear analysis. *Computer Methods in Applied Mechanics and Engineering* 2002; **191**(11-12):1129–1157.
20. Brun M, Batti A, Limam A, Gravouil A. Explicit/implicit multi-time step co-computations for blast analyses on a reinforced concrete frame structure. *Finite Elements in Analysis and Design* 2012; **52**:41–59.
21. Boucard PA, Odièvre D, Gatuingt F. A parallel and multiscale strategy for the parametric study of transient dynamic problems with friction. *International Journal of Numerical Methods in Engineering* 2011; **88**:657–672.
22. Ghanem A, Torkhani M, Mahjoubi N, Baranger TN, Combescure A. Arlequin framework for multi-model, multi-time scale and heterogeneous time integrators for structural transient dynamics. *Computational Methods in Applied Mechanics and Engineering* 2013; **254**:292–308.
23. Gendre L, Allix O, Gosselet P, Comte F. Non-intrusive and exact global/local techniques for structural problems with local plasticity. *Computational Mechanics* 2009; :233–245.
24. Passieux JC, Réthoré J, Gravouil A, Baietto MC. Local/global non-intrusive crack propagation simulation using a multigrid X-FEM solver. *Computational Mechanics* 2013; **52(6)**:1381–1393.
25. Plews J, Duarte CA, Eason T. An improved nonintrusive global-local approach for sharp thermal gradients in a standard fea platform. *International Journal for Numerical Methods in Engineering* 2012; **91**(4):361–397.
26. Gupta P, Pereira JP, Kim DJ, et al. Analysis of three-dimensional fracture mechanics problems: A non-intrusive approach using a generalized finite element method. *Engineering Fracture Mechanics* 2012; **90**:41–64.
27. Chantrait T, Rannou J, Gravouil A. Low intrusive coupling of implicit and explicit time integration schemes for structural dynamics: application to low energy impacts on composite structures. *Finite Elements in Analysis and Design, to appear* 2014; .
28. Bettinotti O, Allix O, Malherbe B. A coupling strategy for adaptive local refinement in space and time with a fixed global model in explicit dynamics. *Computational Mechanics* 2014; **53**:561–574.
29. Whitcomb JD. Iterative global/local finite element analysis. *Computers and Structures* 1991; **40**(4):1027–1031.
30. Guidault PA, Allix O, Champaney L, Navarro JP. A two-scale approach with homogeneisation for the computation of cracked structures,. *Computer and Structures* 2007; **85**(17-18):1360–1371.
31. Gendre L, Allix O, Gosselet P. A two-scale approximation of the schur complement and its use for non-intrusive coupling. *International Journal for Numerical Methods in Engineering* 2011; **87**:889–905.
32. Newmark NM. A method of computation for structural dynamics. *Journal of the Engineering Mechanics Division* 1959; **85**(7):67–94.
33. Guguin G, Allix O, Gosselet P, Guinard S. Nonintrusive coupling of 3D and 2D laminated composite models based on finite element 3D recovery. *International Journal of Numerical Methods in Engineering* 2014; **to appear**.
34. Cocchetti G, Pagani M, Perego U. Selective mass scaling and critical time-step estimate for explicit dynamics analyses with solid-shell elements. *Computers and Structures* 2012; **127**:39–52.
35. Prakash A, Hjelmstad KD. A FETI-based multi-time-step coupling method for newmark schemes in structural dynamics. *International Journal of Numerical Methods in Engineering* 2004; **61**:2183–2204.
36. Mahjoubi N, Gravouil A, Combescure A, Greffet N. A monolithic energy conservating method to couple heterogeneous time integrators with incompatible time steps in structural dynamics. *Computer Methods in Applied Mechanics and Engineering* 2011; **200**:1069–1086.

DOI: 10.1002/nme

37. Allix O. A composite damage meso-model for impact problems. *Composites Science and Technology* 2001; **61**:2193–2205.
38. Andelfinger U, Ramm E. Eas-elements for two dimensional, three-dimensional, plate and shell structures and their equivalence to hr-elements. *International Journal of Numerical Methods in Engineering* 1993; **36**:1311–1337.
39. Taylor RL, Beresford PJ, Wilson. A nonconforming element for stress analysis. *International Journal of Numerical Methods in Engineering* 1976; **10**:1211–1219.
40. Simo JC, Rifai MS. A class of assumed strain methods an the method of incompatible modes. *International Journal of Numerical Methods in Engineering* 1990; **29**:1595–1638.
41. To A, Li S. Perfectly matched multiscale simulations. *Physical Review B* 2005; **72**(035414).
42. Sukumar N, Moës N, Moran B, Belytschko T. Extended Finite Element method for three-dimensional crack modeling. *International Journal for Numerical Methods in Engineering* 2000; **48**(11):1549–1570.
43. Oliver J, Huespe AE, Pulido MDG, Samaniego E. On the strong discontinuity approach in finite deformation settings. *International Journal for Numerical Methods in Engineering* 2003; **56**:1051–1082.
44. Armero F, Linder C. Numerical simulation of dynamic fracture using finite elements with embedded discontinuities. *International Journal of Fracture* 2009; **160**:119–141.

DOI: 10.1002/nme